AGU PUBLICATIONS

JGR

Journal of Geophysical Research: Space Physics

RESEARCH ARTICLE
10.1002/2017JA024189

This article is a companion to *Chen et al.* (2017), https://doi.org/10.1002/2017JA024186.

Key Points:
- The effects of artificially increased kinetic scales are studied with MHD-EPIC simulations
- Changing the kinetic scales does not change the global solution significantly
- Increasing the kinetic scales makes global simulations with embedded kinetic regions feasible

Correspondence to:
G. Tóth
gtoth@umich.edu

Citation:
Tóth, G., Chen, Y., Gombosi, T. I., Cassak, P., Markidis, S., & Peng, I. B. (2017). Scaling the ion inertial length and its implications for modeling reconnection in global simulations. *Journal of Geophysical Research: Space Physics*, *122*, 10,336–10,355. https://doi.org/10.1002/2017JA024189

Received 24 MAR 2017
Accepted 2 SEP 2017
Accepted article online 18 SEP 2017
Published online 21 OCT 2017

Scaling the Ion Inertial Length and Its Implications for Modeling Reconnection in Global Simulations

Gábor Tóth[1], Yuxi Chen[1], Tamas I. Gombosi[1], Paul Cassak[2], Stefano Markidis[3], and Ivy Bo Peng[3]

[1]Center for Space Environment Modeling, University of Michigan, Ann Arbor, MI, USA, [2]Department of Physics and Astronomy, West Virginia University, Morgantown, WV, USA, [3]Department for Computational Science and Technology, KTH Royal Institute of Technology, Stockholm, Sweden

Abstract We investigate the use of artificially increased ion and electron kinetic scales in global plasma simulations. We argue that as long as the global and ion inertial scales remain well separated, (1) the overall global solution is not strongly sensitive to the value of the ion inertial scale, while (2) the ion inertial scale dynamics will also be similar to the original system, but it occurs at a larger spatial scale, and (3) structures at intermediate scales, such as magnetic islands, grow in a self-similar manner. To investigate the validity and limitations of our scaling hypotheses, we carry out many simulations of a two-dimensional magnetosphere with the magnetohydrodynamics with embedded particle-in-cell (MHD-EPIC) model. The PIC model covers the dayside reconnection site. The simulation results confirm that the hypotheses are true as long as the increased ion inertial length remains less than about 5% of the magnetopause standoff distance. Since the theoretical arguments are general, we expect these results to carry over to three dimensions. The computational cost is reduced by the third and fourth powers of the scaling factor in two- and three-dimensional simulations, respectively, which can be many orders of magnitude. The present results suggest that global simulations that resolve kinetic scales for reconnection are feasible. This is a crucial step for applications to the magnetospheres of Earth, Saturn, and Jupiter and to the solar corona.

1. Introduction

Plasma systems are often characterized by large separation of spatial and temporal scales. In the magnetospheres of Earth, Saturn, and Jupiter, or in the solar corona, the ion kinetic scales characterized by the ion inertial length d_i are orders of magnitude smaller than the global scales of the system d_g characterized by the magnetopause standoff distance or some fraction of the solar radius. Electron scales characterized by the electron skin depth d_e are even smaller. Systems with a broad range of temporal and spatial dynamical scales present observational, theoretical, and computational challenges.

In some special cases, for example, shock waves in an ideal neutral gas, the global behavior does not depend on the details of the small-scale physics, because the jump conditions across a hydrodynamic shock are fully determined by the conservation of mass, momentum, and energy. For more complicated systems, such as magnetohydrodynamics with anisotropic ion pressure, the conservation laws constrain the jump conditions, but the pressure anisotropy behind the shock cannot be determined without knowledge of small-scale processes.

Magnetic reconnection is even more complex and challenging. In general, the global dynamics roughly determines the possible locations where reconnection can occur, but reconnection is a dynamic process with complex behavior. Even for the simplest magnetohydrodynamic description of plasma, the energy conservation law only tells us that the magnetic energy will be converted into other forms of energy, but it does not predict, in general, how fast the energy conversion will occur, or how the converted energy will be distributed between bulk kinetic and thermal energies. If we allow for pressure anisotropy and separate electron and ion temperatures, the outcome of the reconnection process is even less determined by simple conservation laws, and more dependent on the small-scale processes.

While magnetic reconnection occurs on the kinetic scales, it is well known that reconnection can globally affect systems of much larger size. Some typical examples are the magnetospheres of planets or the solar corona, where reconnection plays a crucial role in global phenomena, such as magnetic storms and coronal

mass ejections. If we are interested in the interplay between the global plasma system and the reconnection process, it is a natural question to ask how the behavior of the system depends on the ratio d_g/d_i. Clearly, if d_g/d_i is a relatively small number (order of 10 or less), the kinetic effects will have a direct impact on the global solution, even if no reconnection occurs. For example, in Ganymede's magnetosphere $d_g/d_i \approx 10$ and indeed the ideal or resistive MHD solutions that neglect the Hall effect are globally different from the Hall MHD (Dorelli et al., 2015) or the magnetohydrodynamics with embedded particle-in-cell (MHD-EPIC) solution (Tóth et al., 2016). On the other hand, if d_g/d_i is a very large number, then the kinetic effects will be mostly limited to the reconnection region. There can be other kinetic effects that may act on a larger scale (for example, foreshock waves and energetic particles), but in this work we concentrate on systems, where the kinetic effects of interest are limited to the reconnection process.

The main question we are going to address in this work is how the coupled global-kinetic system depends on the value of d_g/d_i when it is large versus extremely large, and how we can change this scale separation. Let us examine the various kinetic length scales and see if there is a way to change them. The smallest plasma scale, where significant charge separation may occur, is given by the Debye length (in SI units) as

$$\lambda_D = \sqrt{\frac{\epsilon_0 v_{\mathrm{th},e}^2}{q_e^2 n_e}} = \frac{m_e}{q_e}\frac{\sqrt{\epsilon_0 p_e}}{\rho_e} \tag{1}$$

where m_e is the electron mass, $q_e > 0$ is the elementary charge, n_e and ρ_e are the electron number and mass densities, respectively, ϵ_0 is the permittivity of vacuum, $v_{\mathrm{th},e} = \sqrt{p_e/\rho_e}$ is the electron thermal velocity, and p_e is the electron pressure.

The change of magnetic topology during collisionless magnetic reconnection occurs in the electron diffusion region (Vasyliunas, 1975). For antiparallel reconnection the characteristic size is the electron skin depth

$$d_e = \sqrt{\frac{m_e}{n_e q_e^2 \mu_0}} = \frac{m_e}{q_e}\sqrt{\frac{1}{\rho_e \mu_0}} \tag{2}$$

where $\mu_0 = 1/(c^2\epsilon_0)$ is the magnetic permeability of vacuum and c is the speed of light, so $\lambda_D = (v_{\mathrm{th},e}/c)d_e$. If the electron thermal velocity is much less than the speed of light, the Debye length is much smaller than the electron skin depth. A standard trick to reduce this separation of scales is to artificially reduce the speed of light to a value that is still larger than the thermal and bulk velocities, but not many orders of magnitude larger.

When there is a significant guide field, the electron scales are determined by the electron gyroradius

$$r_e = \frac{v_{\mathrm{th},e} m_e}{q_e B} = \frac{m_e}{q_e}\frac{\sqrt{p_e/\rho_e}}{B} \tag{3}$$

where B is the magnetic field strength. When the electron thermal velocity $v_{\mathrm{th},e}$ equals the electron Alfvén speed $v_{A,e} = B/\sqrt{\mu_0 \rho_e}$, then the electron gyroradius r_e equals the electron skin depth d_e, so in the vicinity of reconnection sites, r_e and d_e are typically comparable.

The characteristic scales for kinetic ion physics are given by the ion inertial length

$$d_i = \sqrt{\frac{m_i}{n_i q_i^2 \mu_0}} = \frac{m_i}{q_i}\sqrt{\frac{1}{\rho_i \mu_0}} \tag{4}$$

and the ion gyroradius

$$r_i = \frac{v_{th,i} m_i}{q_i B} = \frac{m_i}{q_i}\frac{\sqrt{p_i/\rho_i}}{B} \tag{5}$$

These are $\sqrt{m_i/m_e}$ times larger than the corresponding electron length scales d_e and r_e, respectively, assuming that $n_i = n_e$ (which implies $\rho_i/\rho_e = m_i/m_e$), $q_i = q_e$ and $p_i = p_e$. For a proton-electron plasma $d_i/d_e = \sqrt{1,836} \approx 43$. This ratio already presents a daunting challenge to computational models, especially in three dimensions (3-D), since one needs to model hundreds of d_i in each spatial dimension. A standard trick is to artificially reduce the mass ratio to a smaller value, anywhere from 25 and higher. Such a technique is only allowable if using an unrealistic ion to electron mass ratio does not greatly change the reconnection

process. There have been numerous studies (Hesse et al., 1999; Lapenta et al., 2010; Ricci et al., 2004; Shay & Drake, 1998; Shay et al., 2007) that found only a relatively weak dependence of the reconnection process on the mass ratio. In practice almost all numerical studies, especially in 3-D, use a reduced ion-electron mass ratio.

Here we propose to use a similar trick to change the ion and electron scales relative to the global scale d_g. The kinetic length scales defined in equations (1)–(5) are all proportional to the mass to charge ratios m_e/q_e and m_i/q_i. We will therefore increase the ion and electron mass to charge ratios by a kinetic scaling factor f while keeping the MHD quantities, the mass densities ρ_e and ρ_i, the pressures p_e and p_i, the bulk velocities $\mathbf{u}_e$ and $\mathbf{u}_i$, the magnetic field $\mathbf{B}$, and the various constants ϵ_0, μ_0, and c unchanged. Note that the characteristic speeds (bulk velocity, thermal velocity, Alfvén speed) are not affected by the scaling. In fact, the proposed *kinetic scaling* has no effect on ideal or resistive MHD.

As long as the scaled d_g/d_i ratio remains large enough, it is plausible that the global solution might not be sensitive to the actual value of d_i due to the separation of scales. We hypothesize that

1. the solution on the global scales does not depend sensitively on f;
2. the solution on the kinetic scales is similar for different values of f, but the spatial and temporal scales are proportional to f; and
3. structures forming at the kinetic scales and growing to the global scales follow a self-similar growth at the intermediate scales.

In this paper we will conduct numerical experiments to see whether these statements hold true or not and what their limitations are. These numerical experiments require that the model captures both the global and the kinetic scales. With a pure kinetic code the simulations would be computationally extremely expensive, even in two spatial dimensions (2-D). Fortunately, the simulations can be performed with the MHD-EPIC method (Daldorff et al., 2014; Tóth et al., 2016): the MHD model provides the global solution while the embedded PIC model simulates the reconnection region. The MHD model BATS-R-US (Powell et al., 1999; Tóth et al., 2012) employs a block-adaptive mesh refinement (AMR) for the sake of efficiency, while the PIC model is the implicit particle-in-cell code iPIC3D (Markidis et al., 2010) that uses a semi-implicit scheme (Brackbill & Forslund, 1982) to allow larger grid cell sizes and time steps than the explicit PIC algorithms. The MHD and PIC models are efficiently coupled through the Space Weather Modeling Framework (SWMF) (Tóth et al., 2005, 2012, 2016).

Independent of the numerical method employed, the ratio of the global and kinetic scales has a tremendous impact on the computational cost of global simulations that account for kinetic effects. The required grid cell size is proportional to f, so the number of grid cells and macroparticles is proportional to f^{-D}, where D is the number of spatial dimensions. In addition, the time step limited by stability and/or accuracy constraints is also proportional to f, so the computational cost of advancing the simulation to a given simulation time is reduced by a factor of f^3 in 2-D and a factor of f^4 in 3-D. In addition to the theoretical interest in the scaling properties of the reconnection process, these computational benefits are a major motivation of our work. Using the kinetic scaling makes it possible to perform 3-D global simulations of Earth's magnetosphere, while using a kinetic model to capture the reconnection process, as demonstrated in our companion paper by Chen et al. (2017).

In the following sections we will briefly describe the theoretical arguments behind our scaling hypothesis, the numerical models, the simulation setup and then discuss the results of the numerical experiments.

2. Theoretical Arguments

Here we present some theoretical arguments in support of our hypothesis. This is not intended to be a proof, rather, we argue that the scaling is plausible.

2.1. Global Scales: Insensitivity

The main role of magnetic reconnection in the global dynamics of Earth's magnetosphere is to drive magnetospheric convection. The aspect of reconnection that determines the global response is the reconnection rate. In particular, if reconnection is slow or nonexistent, such as for due northward interplanetary magnetic field (IMF) in the absence of a dipole tilt, the magnetospheric response is minimal. If reconnection is present and efficient (such as when the interplanetary magnetic field has a southward component), then the Dungey cycle of magnetospheric convection occurs. Thus, the bare minimum requirement to capture the global-scale response is an accurate representation of the reconnection rate. Similar arguments apply to other global systems that involve reconnecting magnetic fields.

A significant amount of research has gone into determining the reconnection rate for collisionless plasmas. It has been established by several kinetic modeling studies of symmetric antiparallel reconnection in a rectangular two-dimensional domain (Birn et al., 2001; Huba & Rudakov, 2004; Schoeffler et al., 2012; Shay et al., 1999) that the steady state reconnection rate, quantified as the reconnection electric field E, is about 0.1 times the reconnecting magnetic field strength B_r times the Alfvén speed $v_{Ar} = B_r/\sqrt{\mu_0\rho}$ outside the current sheet. Insight on why the normalized reconnection rate $E/(B_r v_{Ar}) \approx 0.1$ seems to be independent of system parameters has only been achieved recently (Liu et al., 2017).

At the dayside magnetopause, the reconnection is asymmetric with different magnetic field strengths, densities, and temperatures on the two sides of the reconnection region. It was shown that the asymmetric reconnection rate, in 2-D antiparallel reconnection in a rectangular domain, is also 0.1 when normalized to a suitably defined hybrid Alfvén speed and magnetic field (Cassak & Shay, 2007). There is also observational support for this prediction (Mozer & Hull, 2010).

Thus, both for symmetric and asymmetric reconnection, the reconnection rate is expected to be of the form $E \sim 0.1 v_{Ar} B_r$. This is important for the present study, because both B_r and the Alfvén speed v_{Ar} are purely MHD-scale quantities that are not affected by the kinetic scale governed by f. In other words, the reconnection rate is not sensitive to f, and therefore the overall global-scale solution will be insensitive to f.

The other important product of reconnection that can affect global dynamics is the production of magnetic islands. This process starts with the tearing instability. The growth rate of the individual islands depends on the reconnection rate. In addition, the islands may coalesce and merge. The interaction of magnetic islands is a complex and somewhat chaotic process for an infinite (e.g., Harris type) current sheet, because in that system there is no global scale along the current sheet (other than the size of the simulation box) that would organize the dynamics. The situation is different when the current sheet has a finite length, because it is part of a global system and there is significant plasma flow along the current sheet.

In the dayside magnetosphere, for example, the curvature of the magnetopause and the magnetosheath flows has a strong influence on the motion of the magnetic islands, or in magnetospheric terms, the flux transfer events (FTEs). The FTEs are swept either northward or southward by the bulk flow, and their growth stops when they reach the end of the current sheet at the cusps. Similarly, in the magnetotail, the overall plasma convection will push the magnetic islands, often called plasmoids, either tailward or planetward, and their time to grow is limited by the extent of the tail current sheet.

The reconnection rate governing the growth rate, and the plasma flow speed and the extent of the current sheet determining the lifetime of the magnetic islands are independent of the kinetic scaling factor f; therefore, we expect the global dynamics to be insensitive to the value of f.

2.2. Kinetic Scales: Proportionality

If we place ions and electrons into a box, the spatial scale of the various structures formed by them will depend on the electron and ion scales (λ_D, d_e, r_e, d_i, and r_i) and the initial and boundary conditions.

Kinetic simulations often employ periodic boundary conditions. If the computational domain is large enough and the initial conditions do not have any scales, for example, the plasma has uniform density, pressure, and velocity and the magnetic field is also constant, then the solution will scale purely with the electron and ion length scales that are all proportional to the mass per charge ratios m_e/q_e and m_i/q_i. The same holds if the initial conditions are not uniform but contain a discontinuity, such as a sharp current sheet, because a discontinuity does not introduce any length scale. In fact, most kinetic simulation results are presented in length units normalized to d_i and time normalized to the inverse of the ion cyclotron frequency. Of course, one may introduce a global scale into the system through the initial conditions, but here we are interested in structures formed spontaneously by the reconnection process, and the size of those structures will scale with the kinetic length scales.

When the box is part of a global system, the boundary conditions applied to the box will have an influence. We assume that the boundary conditions are well described by MHD quantities, so the deviations from a Maxwellian distribution are relatively small at the boundaries. In the simplest case the boundary conditions are homogeneous (constant density, velocity, pressure, and magnetic field), so no global scales are introduced into the system. A slightly more complicated example is when there is a discontinuity in the boundary conditions, for example, a current sheet. Again, no global length scale is introduced. In the most general case, of course, the boundary and initial conditions will have gradients and higher derivatives that introduce a global

scale d_g. Our hypothesis states that as long as $\epsilon = d_i/d_g$ is much smaller than 1, the spatial scales of the reconnection dynamics will be predominantly determined by d_i and d_e and will not be sensitive to d_g.

2.3. Intermediate Scales: Self-Similarity

We argued in the previous two subsections that the global dynamics are determined by MHD quantities, while the kinetic scales are proportional to f. What about structures that start at the kinetic scales and grow to the global scales? For example, magnetic islands (flux transfer events, plasmoids) are initiated at the kinetic scale that is proportional to f, and they grow in size to the global scales. Depending on f, the FTEs will be at different stages of their evolution (characterized by their size s relative to d_i) when they reach the global scale ($s \propto d_g$). The only way these structures will look similar at the global scale is if their evolution is self-similar at the intermediate scales.

Self-similar solutions arise naturally for PDEs that have no inherent length and time scales. If the initial conditions do not define a length scale, for example, it consists of two uniform states separated by a discontinuity (shock tube problems), the solution will be self-similar. The Euler equations and the ideal MHD equations are two examples for PDEs without any inherent length or time scales. The Navier-Stokes equations have an inherent length scale due to viscosity, and similarly, the Hall MHD equations have an inherent length scale of the ion inertial length. As long as these are very small, we may expect that the evolution will become self-similar once the size s is much larger than the kinetic scale d_i but still small relative to the global scales d_g. For the Vlasov equations there are two inherent length scales, the ion scales characterized by d_i and the electron scales given by d_e, but the above argument still applies as long as the ratio $d_i/d_e = \sqrt{m_i/m_e}$ is kept constant while changing f, or if they are also well separated: $d_i \gg d_e$.

In the collisionless reconnection process multiple magnetic islands of different sizes form near each other, they interact with each other and often merge to form larger islands. This is a much more complicated process than the growth of an individual island. Still, it is plausible to assume that the end result of these interactions at a fixed intermediate scale will look similar independent of the scaling of the much smaller kinetic scales. Similar ideas of self-similar plasmoid-driven reconnection have been suggested and numerically studied by Nitta et al. (2002), Schoeffler et al. (2012), Shibata & Tanuma (2001), and Tenerani et al. (2015).

3. MHD-EPIC Model

The magnetohydrodynamics with embedded PIC algorithm (MHD-EPIC) (Daldorff et al., 2014) couples an MHD and a PIC model both ways. First, the MHD model produces a solution in the full computational domain that covers the global system. Next, one or more PIC regions are selected based on the sites of interest, such as reconnection sites. The PIC model is initialized with the MHD solution in the PIC regions by generating macro-particles with the proper mass density, velocity, and pressure assuming Maxwellian distribution functions. From this point on, the PIC model solves the Vlasov-Maxwell equations as usual, and the MHD solution is completely overwritten inside the PIC regions based on the moments of the distribution functions obtained by the PIC model. The boundary conditions of the PIC model are provided by the MHD model at the boundaries of the PIC regions that are placed far enough from the reconnection sites so that the MHD approximation is valid. The MHD and PIC models exchange information periodically until the simulation is stopped. The coupling is performed in an efficient manner using parallel message passing through the SWMF. The BATS-R-US grid blocks that interact with the PIC region(s) are distributed evenly among the processors to improve the load balance. Typically, the coupling uses only a few percent of the total computational time.

The original MHD-EPIC algorithm (Daldorff et al., 2014) has been extended in several ways:

1. The MHD and PIC grids do not need to be aligned or have the same resolution.
2. The MHD grid can be non-Cartesian.
3. The MHD and PIC models may take different time steps.
4. Multispecies and multi-ion (Hall) MHD can be coupled with the PIC model.

The first two improvements allow more flexibility in the choice of the spatial discretization for the MHD model and also in the placement of the PIC region in the global domain. The third improvement makes the model more robust as it allows both models to adjust their time steps based on their respective stability and/or accuracy conditions. In fact, the iPIC3D code now has the option to adjust its time step based on the electron particle velocities and the cell size as $\Delta t_{\mathrm{PIC}} = C \min(\Delta s_{\mathrm{PIC}}/v_{e,\mathrm{rms}})$ where Δs_{PIC} is the smallest dimension of the PIC grid cells and $v_{e,\mathrm{rms}}$ is the root-mean-square of the macroparticle electron velocities calculated

in each PIC grid cell. The minimum is taken over all the PIC grid cells. The C coefficient should be less than one to maintain accuracy. We set $C = 0.4$ in all simulations. The BATS-R-US code also sets the time step based on the stability conditions. The coupling frequency is usually set to be close to the typical value of the larger of the MHD and PIC time steps.

The last improvement means that the MHD-EPIC model now allows the MHD code to solve the multispecies, multi-ion and two-fluid MHD equations. In this work BATS-R-US solves the two-fluid equations, that is, the Hall MHD equations together with a separate electron pressure equation:

$$\frac{\partial \rho}{\partial t} + \nabla \cdot (\rho \mathbf{u}) = 0 \tag{6}$$

$$\frac{\partial \rho \mathbf{u}}{\partial t} + \nabla \cdot \left[\rho \mathbf{u}\mathbf{u} + I \left(p + p_e + \frac{B^2}{2\mu_0} \right) - \frac{\mathbf{B}\mathbf{B}}{\mu_0} \right] = 0 \tag{7}$$

$$\frac{\partial \mathbf{B}}{\partial t} + \nabla \times \mathbf{E} = 0 \tag{8}$$

$$\frac{\partial e}{\partial t} + \nabla \cdot \left[\mathbf{u} \left(\frac{1}{2}\rho u^2 + \frac{\gamma p}{\gamma - 1} \right) + \mathbf{u}_e p_e + \frac{\mathbf{E} \times \mathbf{B}}{\mu_0} \right] = p_e \nabla \cdot \mathbf{u}_e \tag{9}$$

$$\frac{\partial p_e}{\partial t} + \nabla \cdot (p_e \mathbf{u}_e) = -(\gamma - 1) p_e \nabla \cdot \mathbf{u}_e \tag{10}$$

where I is the identity matrix, $\gamma = 5/3$ is the adiabatic index both for ions and electrons, ρ, $\mathbf{u}$, and p are the mass density, bulk velocity, and pressure of ions,

$$\mathbf{u}_e = \mathbf{u} - \frac{\mathbf{J}}{q_e n_e} = \mathbf{u} - \frac{m_i}{q_i} \frac{\mathbf{J}}{\rho} \tag{11}$$

is the electron velocity, $\mathbf{J} = \nabla \times \mathbf{B}/\mu_0$ is the current density,

$$\mathbf{E} = -\mathbf{u}_e \times \mathbf{B} - \frac{\nabla p_e}{n_e q_e} + \eta \mathbf{J} = -\mathbf{u} \times \mathbf{B} + \frac{m_i}{q_i} \frac{\mathbf{J} \times \mathbf{B} - \nabla p_e}{\rho} + \eta \mathbf{J} \tag{12}$$

is the electric field, η is the resistivity, and

$$e = \frac{p}{\gamma - 1} + \frac{\rho u^2}{2} + \frac{B^2}{2\mu_0} \tag{13}$$

is the total ion plus magnetic energy density. Note that the electron thermal energy is not included, which explains the source term on the right-hand side of equation (9). This choice does not affect the energy conservation properties, since the sum of the energy equation (9) and $1/(\gamma - 1)$ times the electron pressure equation (10) gives the total energy conservation law with no source terms both analytically and in the discretized form. Note that the electron-ion energy exchange term is ignored for this collisionless plasma. In fact, collisional resistivity is also zero in reality, and we only use it for setting up the initial conditions as discussed in the next section.

4. Numerical Schemes

In the simulations presented here, BATS-R-US uses the second-order total variation diminishing scheme (van Leer, 1979) with Rusanov flux function (Rusanov, 1962) and Koren's limiter (Koren, 1993) with the parameter $\beta = 1.2$. The initial conditions are obtained with BATS-R-US only by solving the resistive MHD equations with a constant magnetic diffusivity $\eta/\mu_0 = 10^{10}$ m^2/s applied in the induction equation. The only goal of using resistivity is to make the current sheets smooth and stable (no islands); therefore, the Joule heating and the heat exchange terms between the electrons and ions are switched off to avoid unwanted heating of the electrons and thermal equilibration between the ions and electrons. We run BATS-R-US in local time stepping mode (Tóth et al., 2012) for 10,000 iterations to reach the steady state.

The time-dependent simulations start from this initial steady state solution. BATS-R-US solves the two-fluid MHD equations with the Hall and electron pressure gradient terms in the induction equation, but no resistivity. To avoid the time step limitation due to the whistler waves, a semi-implicit time discretization is used for the Hall term. The numerical diffusion due to the whistler speed is reduced by a factor of 10 similar to the reduction used in the fully implicit Hall MHD scheme (Tóth et al., 2008).

We use the eight-wave scheme (Powell, 1994) in combination with hyperbolic/parabolic cleaning (Dedner et al., 2003) to control the numerical divergence of the magnetic field. Usually, the eight-wave scheme is sufficient in pure MHD and Hall-MHD simulations, but for MHD-EPIC there is a problem: the divergence error (that is advected by the eight-wave scheme together with the plasma) cannot propagate through the PIC region, since iPIC3D does not use the eight-wave scheme. As a result, the divergence errors can accumulate at the boundary of the PIC region. Using the hyperbolic/parabolic cleaning helps, because it can dissipate the divergence error in all directions, not only along stream lines. We set the hyperbolic speed parameter to $c_h = 400$ km/s and the parabolic decay parameter to $c_p = 0.1$ (see Dedner et al., 2003 and Tóth et al., 2012).

The iPIC3D code solves the Maxwell equations for the electric and magnetic fields and the equations of motion for the particles as usual (Markidis et al., 2010). It uses an implicit scheme (Brackbill & Forslund, 1982) to solve for the electric field to avoid the numerical stability issues that restrict the cell size Δx to be less than the Debye length λ_D and the time step Δt to be smaller than $\Delta x/c$ (the time it takes for light wave to cross a grid cell) in explicit PIC codes. Even for a semi-implicit PIC code, using the true speed of light, while possible, is computationally expensive, because it makes the linear problem to be solved stiffer, requiring more iterations. It is therefore standard practice to artificially lower the speed of light c to a reduced value c' that is still large relative to the flow speeds. This trick, also used in MHD codes (named the semirelativistic or Boris correction, Boris, 1970; Gombosi et al., 2002) exploits the separation of scales between the speed of light and the speed of the plasma flow speeds. In these simulation we used $c' = 3,000$ km/s. To reduce the scale separation of the electron skin depth and ion inertial length, the ion-electron mass ratio is set to $m_i/m_e = 100$. In all simulations each PIC grid cell is initialized with 225 ion and 225 electron macroparticles, and the same number of particles are generated in the PIC grid ghost cells during the MHD-EPIC coupling.

We also find it useful to suppress some short wavelength oscillations that are generated in the PIC region. These oscillations appear to be related to Langmuir waves, and they reach significant amplitudes in 2-D simulations (the issue seems to be less significant in 3-D simulations). A relatively simple way to suppress these waves is the smoothing of the electric field at short wavelengths. After the electric field is obtained by the implicit solver, we apply the following smoothing operator for each grid node indexed by i, j:

$$\mathbf{E}'_{i,j} = \alpha \mathbf{E}_{i,j} + \frac{1-\alpha}{4} \sum_{4 \text{ neighbors}} \mathbf{E}_{i',j'} \tag{14}$$

where the averaging is done over the four immediate neighbors of the cell, while in 3-D the averaging is done for six neighbors. In most of the presented simulations we use $\alpha = 1/2$ and apply five smoothing iterations. In one particular simulation we found that the smoothing caused an instability at the boundary of the PIC domain. To avoid this issue, we have implemented the option to set $\alpha = 1$ at the few cells near the boundary of the PIC region (no smoothing) and only apply the smoothing in the inside:

$$\alpha = \min(1, \alpha_0 + (A - \alpha_0)\max(0, 1 - d/D)) \tag{15}$$

where α_0 is the internal smoothing parameter, d is the distance of the cell from the boundary, and A and D are two constants (we use $A = 2$ and $D = 8\Delta x$). For the sake of consistency, we also smooth the current densities used in the Maxwell solver. We carefully checked that the overall solution is not affected significantly by the smoothing operation other than eliminating the Langmuir patterns.

5. Two-Dimensional Magnetosphere Problem

Our goal is to study the interaction of global and micro scales in a relatively simple system. The two-dimensional (2-D) magnetosphere problem (Daldorff et al., 2014) is well suited: the global scale is set by the interaction of the intrinsic line dipole field and the incoming plasma flow (that we will call the solar wind). A 2-D simulation can be run much faster than a 3-D problem, so we can do a more extended parameter study. In addition, visualization of the 2-D results is much simpler and comprehensive. Of course, the 3-D reconnection dynamics is somewhat different from the 2-D case, but the scaling arguments apply to both. For the sake

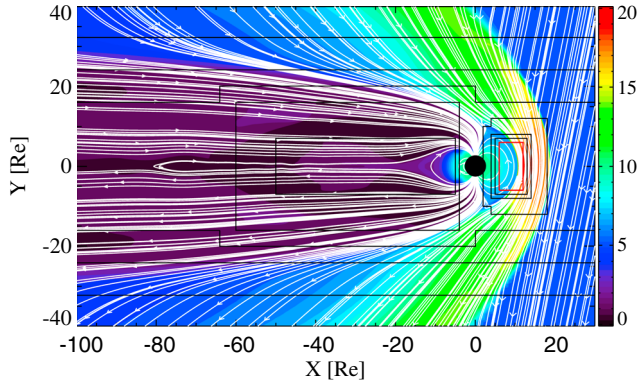

Figure 1. Overview of the initial state after the first 10,000 iterations. Only a part of the computational domain is shown. The colors show density in units of amu/cm^3. The white lines are magnetic field lines, while the black lines represent the grid resolution changes. The red box shows the boundaries of the PIC region.

of easier interpretation, the values are set to be similar to those typical for Earth's magnetosphere. Note, however, that the 2-D simulations are in the magnetic meridional plane, so the Y axis is aligned with the dipole and the Z direction is normal to the plane of the simulation, which is the opposite of the usual 3-D case.

The 2-D domain extends from $x = -480\,R_E$ to $x = 32\,R_E$ and from $y = -128\,R_E$ to $y = 128\,R_E$ (where $R_E = 6,380$ km is the radius of the Earth) with the magnetized planet at the origin. The inner boundary condition is set at a circle of radius 2.5 R_E with a fixed plasma density of 10 amu/cm^3 and zero velocity. The radial component of the magnetic field is set to the line dipole value. The tangential components of the magnetic field and the ion and electron pressures have zero gradient boundary conditions. The line dipole is aligned with the Y axis and its strength is set to −3,110 nT at the magnetic equator. This is 10 times weaker than the 3-D dipole strength of the Earth, but the line dipole field decays with r^{-2} instead of the r^{-3} of the 3-D dipole, so the magnetopause ends up to be at about the same distance (10 R_E) as for Earth's magnetosphere.

The solar wind enters from the $+X$ direction with mass density 5 amu/cm^3, speed −400 km/s, and total pressure 0.031 nPa, of which the electrons have 0.0248 nPa. The electron pressure dominates the pressure of the incoming plasma, but behind the bow shock the ion pressure becomes dominant (by about a factor of 2), because the bow shock is modeled with the MHD code, so the heating of the electrons and ions is determined by the MHD conservation laws. The shock predominantly heats the ions as the bulk kinetic energy is transformed into ion thermal energy (see equations (9) and (13), while the electrons only heat up adiabatically according to equation (10).

The boundary conditions at $y = \pm 128$ are also set to the fixed solar wind parameters. At this distance the solar wind is only slightly perturbed by the interaction with the magnetosphere, so fixed boundary conditions work well. Finally, a zero gradient outflow boundary condition is applied at $x = -480\,R_E$. The outflow boundary has to be placed far away to avoid numerical problems due to the subfast magnetosonic flow behind the bow shock.

The interplanetary magnetic field (IMF) carried by the solar wind is either set to $\mathbf{B} = (-0.1, -0.5, 0)$ nT or $\mathbf{B} = (-0.1, -0.5, -3)$ nT. The Y component is the most important, as it reconnects with the dipole field of the body, which is aligned with the Y axis. In 2-D the IMF cannot slip around the magnetosphere, so the magnetic field has to reconnect at the same average rate as it enters into the system. The $B_y = -0.5$ nT value is selected to yield (a slowly decreasing) magnetopause distance at around 10 R_E. The B_x component is small, but it is set to a nonzero value to break the "north-south" symmetry. If it is set to zero, the Hall MHD simulations produce very large islands at the subsolar point of the magnetopause that can grow to unreasonable size before finally starting to move to the $\pm Y$ direction. Finally, the B_z component controls the amount of guide field at the reconnection site. The $B_z = 0$ choice produces pure antiparallel reconnection with no guide field, while the $B_z = -3$ nT value creates a moderate guide field. Although the IMF magnitude of $|B_z| = 3$ nT is much larger than the IMF magnitude of $|B_y| = 0.5$ nT, near the magnetopause they become comparable. This happens because of the 2-D geometry. At the bow shock both components get amplified by the shock compression ratio, which is close to 4 for this strong shock, so $|B_y|$ and $|B_z|$ become about 2 nT and 12 nT, respectively. In the magnetosheath, however, $|B_y|$ gets further amplified to about 15 nT due the deceleration in the X direction, while B_z is simply advected around the obstacle. The reason is that the flow deflects from the $-X$ to the $\pm Y$ direction in an approximately incompressible manner, which enhances B_y but not B_z. In the end, the guide field B_z becomes comparable to the reconnecting field B_y on the sheath side of the reconnection.

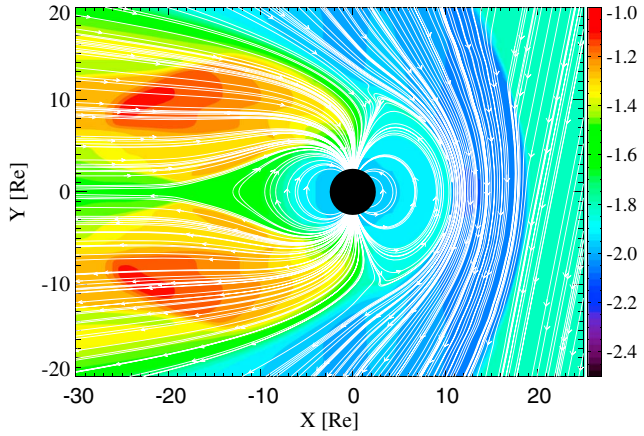

Figure 2. The base 10 logarithm of the inertial length measured in R_E for protons.

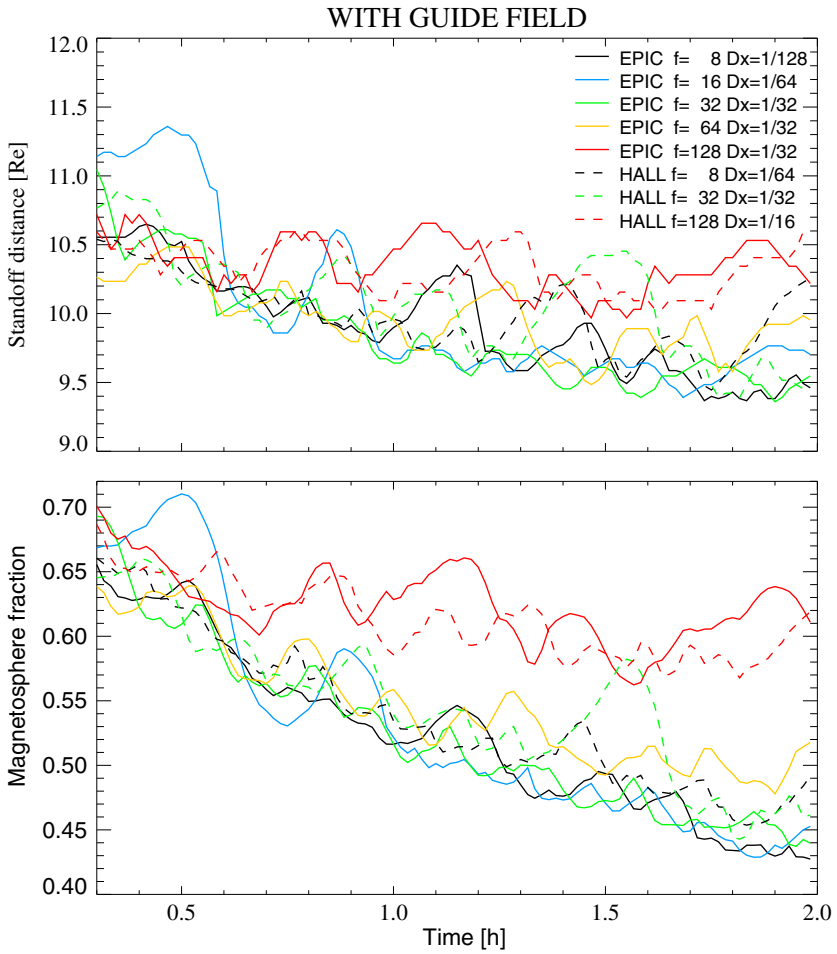

Figure 3. Time series of the (top) standoff distance and the (bottom) volume fraction of the magnetosphere inside the PIC region for several MHD-EPIC and Hall MHD simulations. The kinetic scaling factors (f) and the grid resolutions (Dx) are indicated in the figure legend. All simulations used IMF $B_Z = -3$ nT.

With these parameters, the dayside reconnection site is at the nose of the magnetopause centered at around $x = 10\,R_E$ and $y = 0$ as shown in Figure 1. In BATS-R-US we solve for the Hall term in the "Hall region" placed at $5\,R_E < x < 20\,R_E$ and $-15\,R_E < y < +15\,R_E$ with a smooth tapering at the edges. Limiting the region where the Hall term is used improves computational efficiency without any significant effect on the results around the reconnection site.

In the MHD-EPIC simulations, the PIC region (indicated by the red rectangle in Figure 1) is positioned at $6\,R_E < x < 12\,R_E$ and $-6\,R_E < y < +6\,R_E$, which covers the reconnection site but avoids getting very close either to the body where the plasma beta is very low, or to the bow shock. Note that the PIC region is fully covered by the Hall region, so the Hall effect is taken into account on both sides of the boundaries of the PIC region.

To assess the required grid resolution, we plot the base 10 logarithm of the proton ion inertial length $d_{i,p}$ in units of R_E in Figure 2 for the initial conditions. Near the dayside reconnection site $d_{i,p} \approx 0.01\,R_E$, which means that $d_e \approx 0.001\,R_E$ for the $m_i/m_e = 100$ mass ratio. Resolving the electron scales at least marginally would require $\Delta x \approx d_e$, which would make the PIC region resolved by $6,000 \times 12,000 = 72$ million grid cells and 450 times that many macroparticles, or about 32 billion in total. While this is still doable in 2-D, it is a very expensive calculation and in fact the electron scales are still only marginally resolved. In three spatial dimensions things get clearly unfeasible.

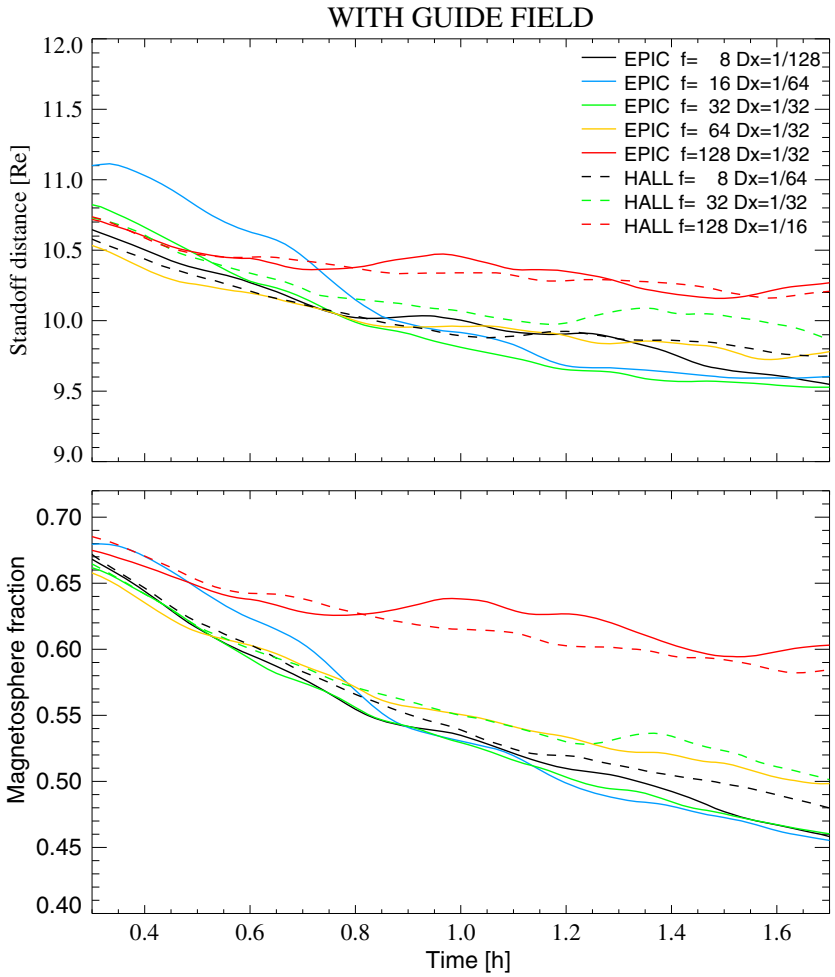

Figure 4. Time series of the (top) standoff distance and the (bottom) volume fraction of the PIC region occupied by magnetospheric plasma for several MHD-EPIC and Hall MHD simulations smoothed with a 30 min boxcar averaging. The simulations used IMF $B_Z = -3$ nT.

Our numerical experiments require that d_i/d_g be a small number, but it is not necessary to start from $d_i = d_{i,p}$ corresponding to $f = 1$. To make the computations affordable, the smallest scaling factor will be set to $f = 8$, which makes $d_i/d_g = f * d_{i,p}/d_g \approx 0.008$, clearly still much less than unity. Correspondingly, the finest grid resolution in the PIC region will be set to $\Delta x = 1/128\, R_E$. The corresponding PIC grid is $768 \times 1,536$ with about 530 million macroparticles.

6. Simulations

We perform two-fluid and MHD-EPIC simulations with grid resolutions Δx varied from $1/128\, R_E$ to $1/16\, R_E$ and scaling factors f varied between 8 and 128. For the two-fluid simulations Δx refers to the MHD grid resolution around the reconnection site, and f is the ion mass per charge m_i/q_i in the Hall term in Ohm's law (equation (12). In the MHD-EPIC simulations Δx is the grid resolution of the PIC model and f is the scaling factor applied to the ion and electron mass per charge ratios. The only other quantity that is varied is the out-of-plane B_z component of the solar wind that is either 0 (no guide field) or -3 nT (guide field). We will present results from the simulations with the guide field unless otherwise noted.

All simulations are initialized with a steady state solution obtained with the resistive MHD equations; however, the grid resolution around the dayside reconnection site varies from $\Delta x = 1/16$ to $1/128\, R_E$, which means that the initial conditions are similar but not necessarily identical. All simulations are run for 2 h, which is sufficient to reach the quasiperiodic formation of magnetic islands, also called flux transfer events (FTEs).

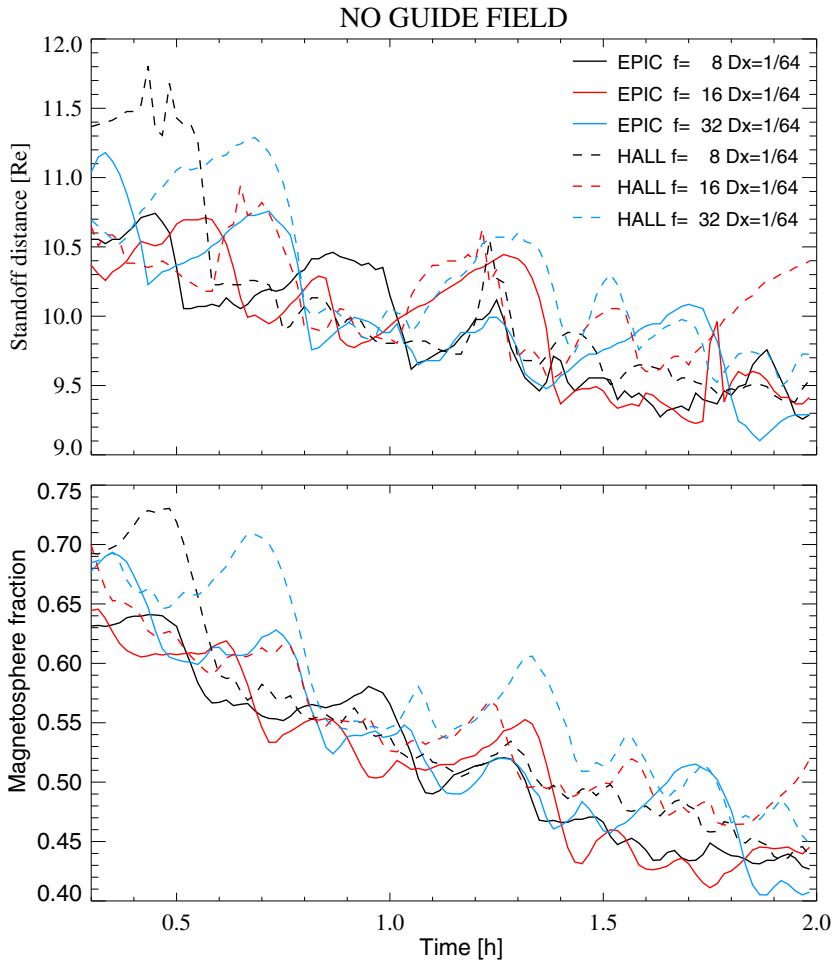

Figure 5. Time series of the standoff distance and the volume fraction of the PIC region occupied by magnetospheric plasma for several MHD-EPIC and Hall MHD simulations. There is no guide field: IMF $B_Z = 0$.

6.1. Global Scales

One of the most characteristic length scales of a magnetosphere is the standoff distance. This is usually estimated to be a position along the $+X$ axis, where the magnetic pressure of the (compressed) dipole field balances the ram pressure of the solar wind. The issue is more complicated in two spatial dimensions, because the Y component of the magnetic field entering with the solar wind has no other way to get to the other side of the planet than magnetic reconnection. If the reconnection rate is too slow, the field will pile up outside the magnetopause. If the reconnection rate is too fast, it will erode the magnetopause too quickly.

We selected the line dipole strength and B_Y to form a magnetopause with about the same standoff distance as found in Earth's 3-D magnetosphere. During the time-dependent simulation the standoff distance is slowly decreasing on average. In addition, there are oscillations related to the large-scale dynamics of the reconnection process. Comparing the time variation of the standoff distance for the simulations using different kinetic scaling factors provides a simple quantitative assessment of their similarities and differences. We use the following simple formula to calculate the standoff distance automatically from the solution on the discrete grid:

$$S = \max_{\{i,j:B_{Y,ij}>3\,\mathrm{nT}\}} x_{ij} \tag{16}$$

where i, j are the indexes of the grid cells. This works well, since $B_Y < 0$ in the solar wind and behind the bow shock, and it is positive inside the magnetopause near the subsolar point. The threshold value of 3 nT was selected so that small B_Y perturbations upstream of the magnetopause are ignored.

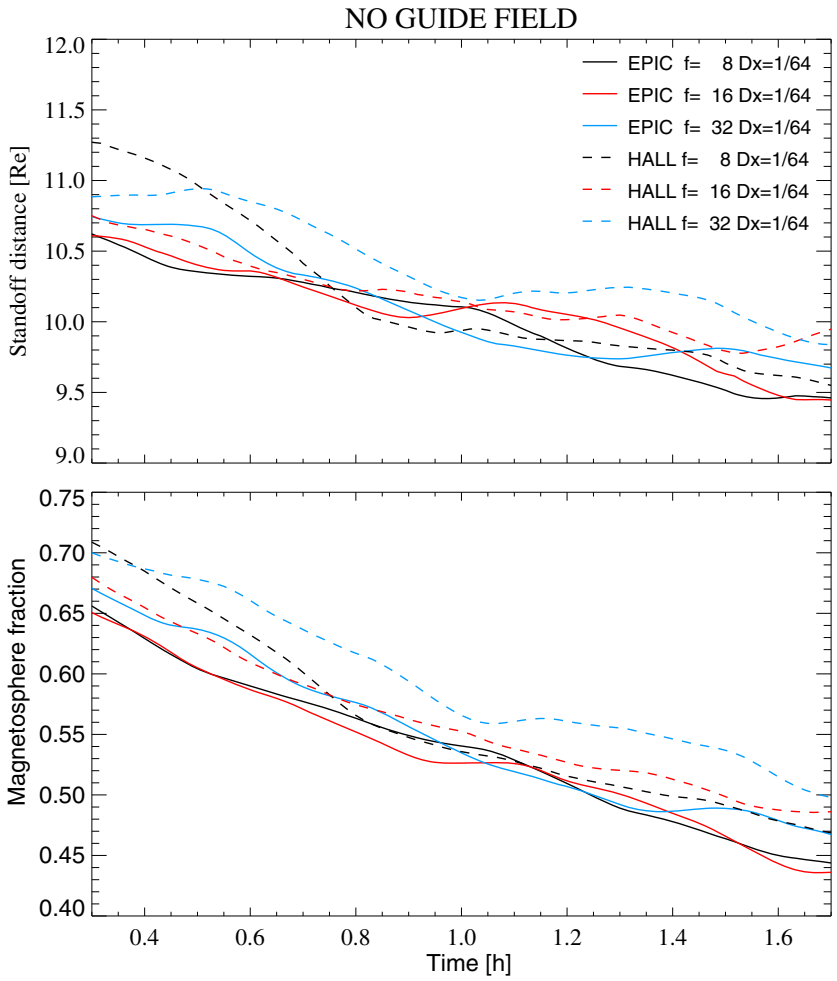

Figure 6. Time series of the standoff distance and the volume fraction of the PIC region occupied by magnetospheric plasma for several MHD-EPIC and Hall MHD simulations smoothed with a 30 min boxcar averaging. There is no guide field: IMF $B_Z = 0$.

Another simple measure for the size of the dayside magnetosphere is the fraction of volume where B_Y is positive around the dayside magnetopause. For the sake of simplicity we use the grid cells inside the PIC region ($6\,R_E < x < 12\,R_E$and $-6\,R_E < y < 6\,R_E$) and define

$$F = \frac{1}{A} \sum_{\{i,j:B_{Y,ij} > 3\,\mathrm{nT}\}} \Delta A_{ij} \tag{17}$$

where ΔA is the size of the grid cell and $A = 72\,R_E^2$ is the total area of the region. This measure is less sensitive to the local variations than the standoff distance, but for the sake of simplicity we use the same threshold value 3 nT.

Figures 3 and 4 show the time series of the standoff distance S and the volume fraction of the magnetosphere inside the PIC region F. Figure 3 provides the values with a 1 min cadence between $t = 0.3$ and $t = 2$ h. Figure 4 shows the same quantities smoothed with a 30 min wide boxcar averaging. Both quantities get smaller with time, which means that the reconnection is eroding the magnetopause and the magnetosphere slowly shrinks. Simulations with $f = 128$ are clearly different from the others in both figures. This is expected, since in this case the separation of kinetic and global scales is not large anymore: $\varepsilon = f d_{i,p}/d_g \approx 128 \times 0.01/10 = 0.128$.

At first glance, the rest of the simulations with $f \leq 64$ look similar when the unsmoothed curves are compared. The smoothed magnetosphere fraction curves (Figure 4, bottom), however, clearly reveal that the Hall MHD simulations (dashed lines) and the MHD-EPIC simulation with $f = 64$ (orange line) significantly deviate

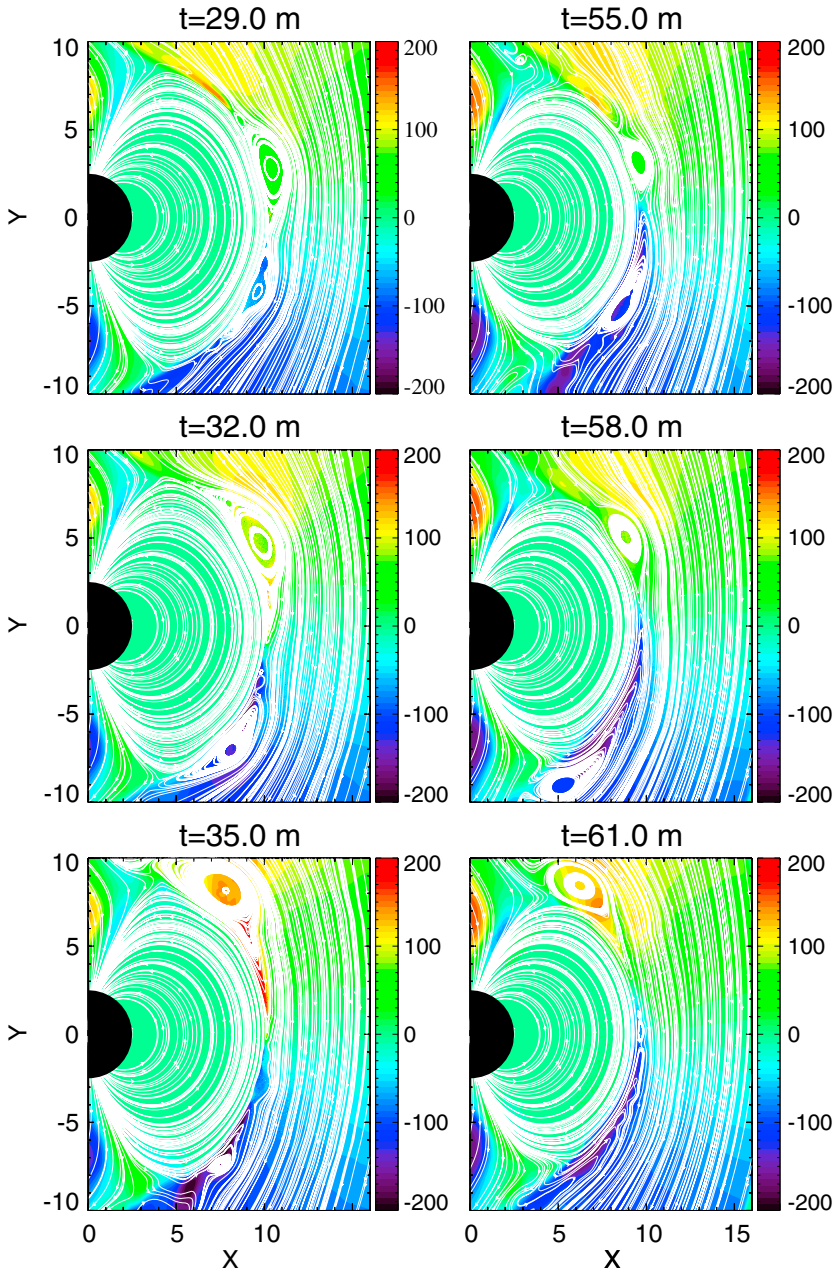

Figure 7. Time series of flux transfer events for two runs: (left column) For kinetic scaling factor $f = 8$ and grid resolution $\Delta x = 1/128\,R_E$; (right column) with $f = 32$ and $\Delta x = 1/32\,R_E$. The simulation times are shown in minutes above each plot with a 3 min cadence. The colors show the Y component of the velocity in km/s units. The white lines are magnetic field line traces.

from the three MHD-EPIC simulations with $f = 8$, 16, and 32 (black, cyan, and green solid lines) which are quite similar to each other overall.

The standoff distance varies more, even with smoothing (Figure 4, top), but the trends are the same: the MHD-EPIC simulations with kinetic scaling factor $f \leq 32$ are closer to each other than the rest of the simulations.

Figures 5 and 6 show results from several simulations with no guide field, that is, the IMF $B_Z = 0$. In these simulations the grid resolution is kept constant at $\Delta x = 1/64\,R_E$, while the kinetic scaling factor is varied between 8 and 32, so all simulations start from the same initial condition. The standoff distance and the magnetosphere fraction without smoothing and with 30 min boxcar smoothing are shown in the figures, respectively.

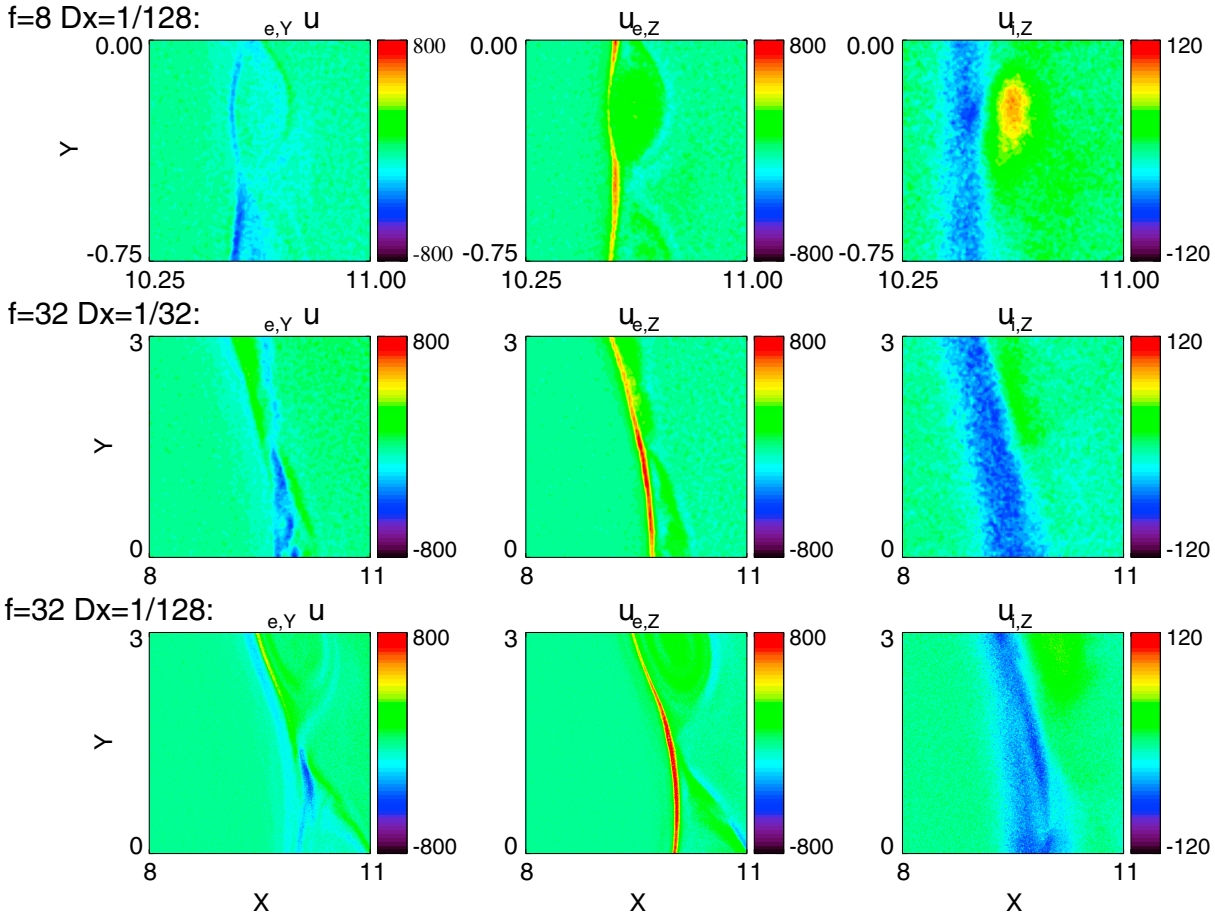

Figure 8. The Y and Z components of the electron velocity and the Z component of the ion velocity in km/s from the iPIC3D output. Three simulations with different f factors and grid resolutions are compared. Note that the spatial scale of the panels in the top row with $f = 8$ is 4 times smaller ($3/4 \times 3/4\, R_E$) than that in the middle and bottom rows with $f = 32$, where the panels are $3 \times 3\, R_E$.

Overall, the decay rates of the standoff distances are similar, but the Hall MHD simulations show some sharp spikes corresponding to $B_y > 3$ nT spots produced by very large FTEs. In contrast the MHD-EPIC simulations show less variation. The volume fraction of the magnetosphere shows smoother variation, as expected. Still, it is clear that the Hall MHD simulations show larger oscillations than the MHD-EPIC solutions. The smoothed curves on Figure 6 show similar trends for all six simulations, although both the standoff distance and the magnetosphere fraction is somewhat larger for the Hall MHD simulations (dashed curves) than for MHD-EPIC (solid curves).

We now focus on the phenomena causing the fluctuations: the large-scale magnetic islands, or FTEs. Figure 7 compares FTEs produced by two MHD-EPIC runs. The simulation shown on the left uses $f = 8$ for the kinetic scaling factor with a $\Delta x = 1/128\, R_E$ grid resolution in the PIC domain, while the one on the right uses $f = 32$ and $\Delta x = 1/32\, R_E$. The three rows correspond to times separated by 3 min. The initial times (29 and 55 min, respectively) are selected so that the FTEs moving toward the $+Y$ direction are roughly at the same stage of evolution. In Figure 7 (top row) the center of the FTEs are roughly at $Y = 3\, R_E$, then 3 min later (Figure 7, middle row) they get to about $Y = 5\, R_E$ and another 3 min later (Figure 7, bottom row) the centers move to about $Y = 8\, R_E$. Overall the size and shape of these flux ropes are very similar. The propagation speed in the Y direction is about $2\, R_E/3$ min ≈ 71 km/s between the initial and midpoint times, and $3\, R_E/3$ min ≈ 106 km/s between the midpoint and final times. These velocities are close to the Y component of the plasma velocity shown by the colors in the figure.

The flux ropes moving in the $-Y$ direction also show similar sizes and shapes, although at this particular time there are multiple flux ropes on the left, and only one dominant flux rope on the right, so their evolution

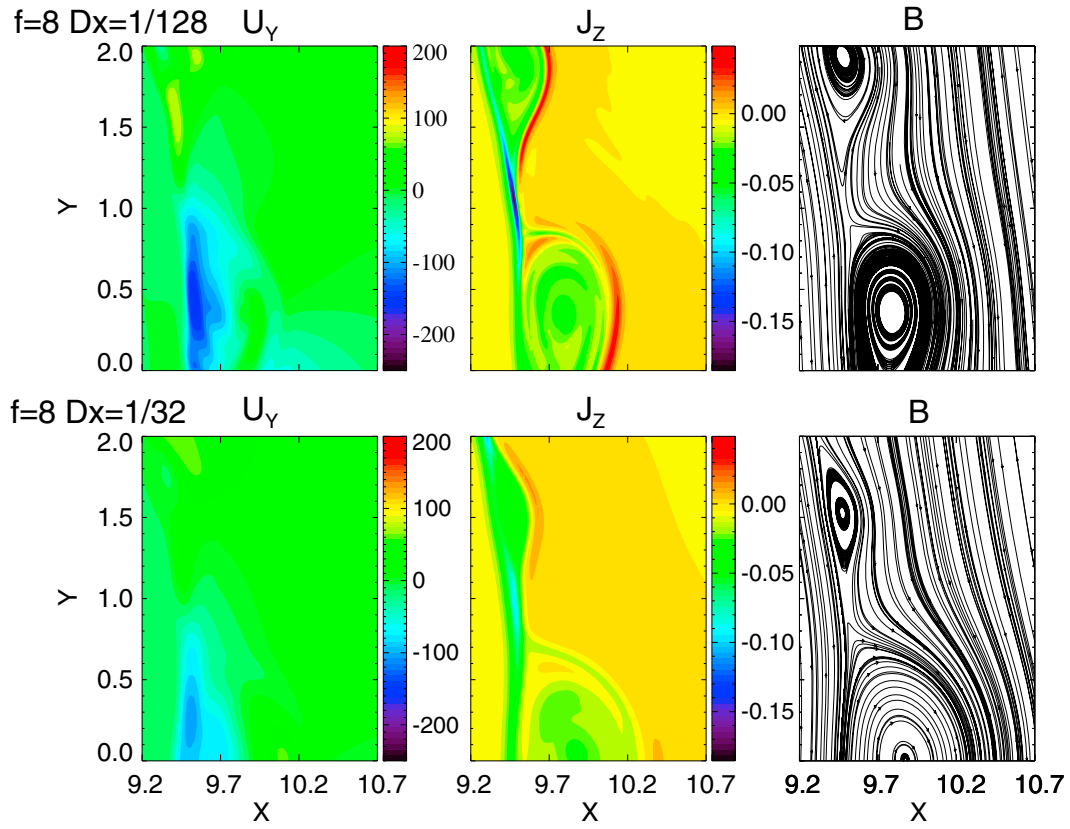

Figure 9. Comparison of the small-scale solutions for two Hall MHD simulations with identical kinetic scaling factors $f = 8$ but different grid resolutions (top row) $\Delta x = 1/128\,R_E$ and (bottom row) $1/32\,R_E$, respectively. The Y component of the ion velocity is in km/s, the Z component of the current in μA, and magnetic field line traces are shown for the same simulation time and same location with similar reconnection events.

is different. The total number and size distribution of flux ropes is also very similar. Looking at animations of multiple simulations side by side indicates that the large-scale FTE dynamics is quite insensitive to the value of the scaling factor f.

6.2. Kinetic Scales

Figure 8 shows the simulation result near the dayside reconnection sites in three simulations with different scaling factors and grid resolutions. The times shown are selected so that the reconnection sites are near the subsolar point of the magnetopause. The Y component of the electron velocity (Figure 8, left column) shows the reconnection jets, while the Z (out-of-plane) component of the electron and ion velocities (Figure 8, middle column and Figure 8, right column) show the current carried by the electrons and ions, respectively. Although the three reconnection sites are from different simulations at different times, the similarities are quite clear. The two simulations with $f = 32$ (Figure 8, middle row and Figure 8, bottom row) are on the same spatial scale, but the grid resolutions are a factor of 4 different. Still, the width of the current sheet near the reconnection site, as indicated by the maxima (red color) of the Z component of the electron velocity are quite similar, around 0.1 R_E or about 3 to 4 d_e, where the electron skin depth is measured on the sheath side of the reconnection site. The width of the ion diffusion regions (shown by the blue regions in Figure 8, right column) is about 1 R_E wide in both cases, which is 10 times wider than the electron diffusion region as expected for the $m_i/m_e = 100$ mass ratio. The electron exhaust jets (Figure 8, left column), although different in detail, also show similar spatial structures and the exhaust velocities have similar values. This suggests that the reconnection dynamics is not dominated by grid resolution effects.

The spatial scales shown for $f = 8$ (Figure 8, top row) are 4 times smaller than the spatial scales shown for the two simulations with $f = 32$. After this visual rescaling the solutions look remarkably similar. The width of the current sheet near the reconnection site (red area in Figure 8, top middle) is about 0.025 R_E that is indeed

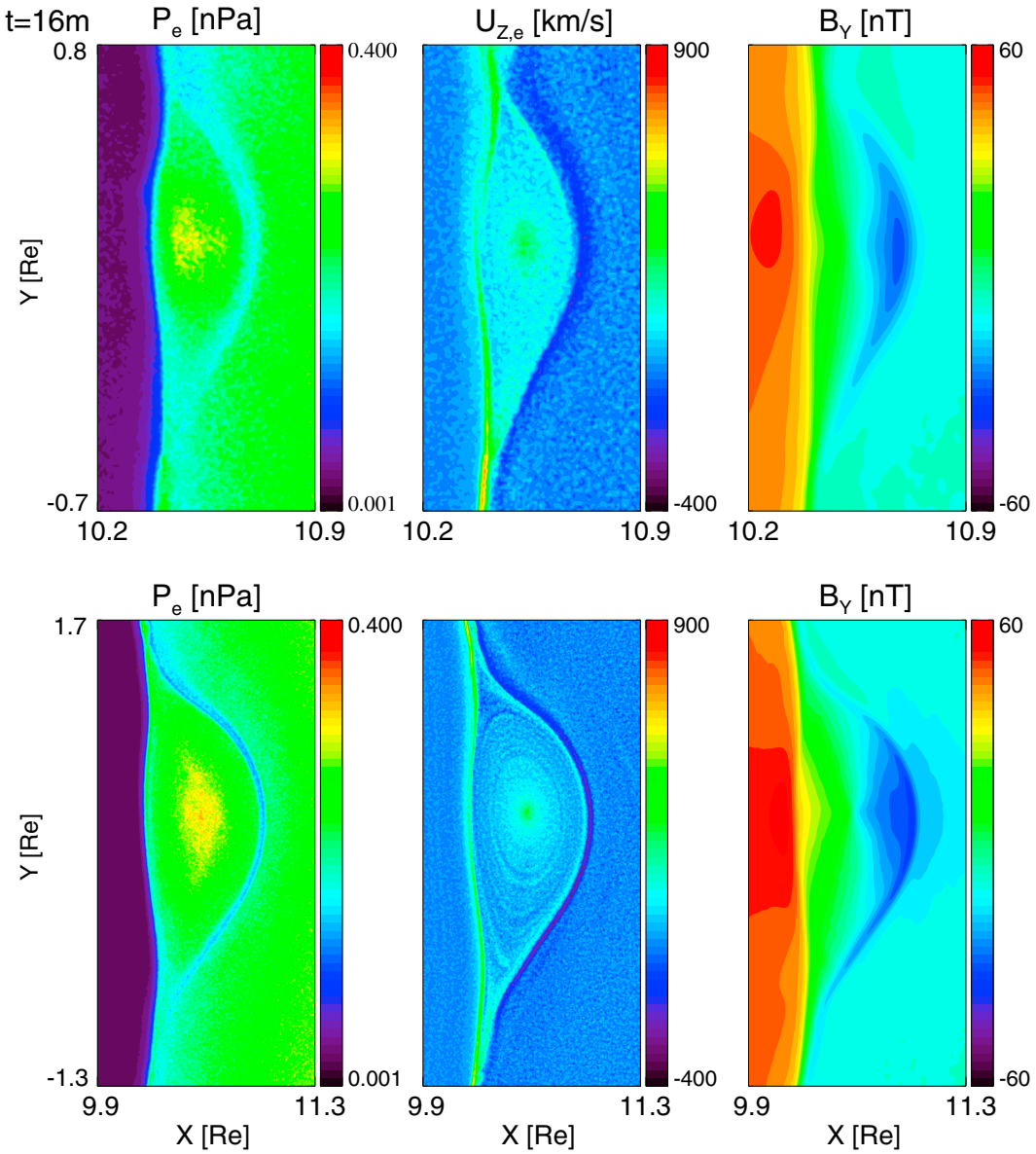

Figure 10. Evolution of an FTE in an MHD-EPIC simulation with scaling factor $f = 8$ and grid resolution $\Delta x = 1/128\, R_E$. The electron pressure, the out-of-plane component of the electron velocity, and the Y component of the magnetic field are shown for time (top row) 16 min and (bottom row) 20 min. The spatial scales are a factor of 2 larger for the later time: the sizes of the panels are $0.7 \times 1.5\, R_E$ and $1.5 \times 3\, R_E$ in Figures 10 (top row) and 10 (bottom row), respectively.

4 times thinner than the current sheets obtained with $f = 32$. The width of the ion diffusion region (blue region in Figure 8, top right) also scales approximately with f. The overall structure and velocity of the reconnection jets is also similar (Figure 8, left column) after the spatial rescaling. These results support the arguments made in section 2.2: the kinetic scales are proportional to f.

In contrast to the PIC solution, in Hall MHD there is no electron scale, so the solution depends, to some extent, on the grid resolution, which determines the numerical dissipation. Figure 9 demonstrates this by comparing two Hall MHD simulations that used the same kinetic scaling factor but grid resolutions differing by a factor of 4. The snapshots are selected to capture magnetic islands of similar sizes and shapes at the same location and time ($t = 76$ min) in the two simulations. While the qualitative pictures are similar, and in fact the magnetic fields are very comparable, there are significant quantitative differences. In Hall MHD the width

of the current sheet is determined by the grid resolution, so it is much thinner on the $\Delta x = 1/128\,R_E$ grid than on the $\Delta x = 1/32\,R_E$ grid. Consequently, the out-of-plane component of the current (determined from $\nabla \times \mathbf{B}$) is much stronger for the higher-resolution run.

6.3. Intermediate Scales

We argued in section 2.3 that the solution should be self-similar at the intermediate scales. Indeed, Figure 10 demonstrates that the growth of an FTE is approximately self-similar. Figure 10 (top row) and Figure 10 (bottom row) show the same FTE at two different times. The panel sizes are $0.7 \times 1.5\,R_E$ for time $t = 16$ m and $1.4 \times 3\,R_E$ for $t = 20$ m. The simulation uses $f = 8$ for the scaling factor, so the kinetic scales are quite small ($d_i \approx 0.08\,R_E$). The grid resolution is $\Delta x = 1/128\,R_E$, so the intermediate and global scales are very well resolved. The FTE was selected based on its formation near the subsolar point, so it stayed roughly at the same place while growing in size. The quantities shown are electron pressure, the out-of-plane component of the electron velocity and the Y component of the magnetic field. We checked that all other quantities show the same behavior.

Comparing the solution at these two times demonstrates that the evolution of an isolated FTE is approximately self-similar at the intermediate scales, which supports our theoretical arguments presented in section 2.3.

7. Conclusions

In many space plasma systems global and kinetic scales are separated by many orders of magnitude; nevertheless, the global system has a major influence on the kinetic processes, and vice versa, the kinetic processes, especially magnetic reconnection, has a major impact on the global dynamics. This scale separation presents a challenge to theoretical, observational, and modeling investigations. The kinetic scales, such as the Debye length, electron skin depth, electron gyroradius, ion inertial length, and ion gyroradius are all proportional to the mass to charge ratio of electrons and ions. We showed that one can artificially change the kinetic scales by changing the ion and electron mass to charge ratios by a scaling factor f while keeping the MHD quantities, such as mass density, pressure, bulk velocity, and magnetic field the same.

We presented a number of theoretical arguments suggesting that as long as the separation between global and kinetic scales remains large enough,

1. the solution of the equations is insensitive to the scaling at global scales, and
2. the solution at kinetic scales will look the same but spatially proportional to the scaling factor.

Our numerical experiments conducted with the MHD-EPIC code show not only that these theoretical expectations are fulfilled but also that the required separation of scales is relatively modest. For the dayside reconnection process the global scale can be characterized by the magnetopause standoff distance, that is, $d_g \approx 10\,R_E$. We found that scaling factors $f \leq 32$ corresponding to the scaled inertial length $d_i \leq 0.32\,R_E$ and $\epsilon = d_i/d_g \leq 0.032$ give very comparable solutions. Further increasing the ion inertial length to $d_i \geq 0.64\,R_E$ and $\epsilon \geq 0.064$, however, produces significantly different results. The simulations also confirmed that the scaled MHD-EPIC simulations provide very similar solutions at the kinetic scales when distance is measured in the ion inertial length d_i that is proportional to the scaling factor f.

In principle, the scaling arguments apply to Hall MHD as well, but in this case the electron scale processes are replaced by numerical and/or some ad hoc resistivity. Assuming that these resistive effects are kept proportional to the grid resolution Δx in a Hall MHD simulation, one would expect that keeping the ratio $d_i/\Delta x$ constant and/or very large is analogous to keeping $d_i/d_e = \sqrt{m_i/m_e}$ constant and/or large in the PIC simulations. Our results suggest that this is approximately true, so Hall MHD simulations can also benefit from the kinetic scaling. We expect that the same is true for hybrid simulations that include the Hall effect.

The scaling of kinetic effects is interesting from a theoretical point of view. The scaling reduces the number of free parameters that enter the system; therefore, results obtained for a given inertial length will have more general applicability. In addition, the scaling and self-similarity may provide insight into the generic properties of collisionless reconnection: distribution of magnetic island sizes, for example, is likely to follow some power laws. Investigating these theoretical consequences is left for future work.

The scaling also has a very practical application, which in fact motivated our research in the first place: increasing the ion inertial length makes kinetic simulations embedded into a global system possible. Resolving

the real ion inertial length in three-dimensional simulations of Earth's magnetosphere is extremely difficult even on the largest available computers. Doing the same in the solar corona is essentially hopeless. To put some numbers behind these statements, let us consider a 3-D global magnetosphere simulation box of $100 \times 100 \times 100\, R_E^3$. An explicit kinetic simulation has to resolve the Debye length that is about 100 m or $\Delta x = 1/64000\, R_E$. The required number of grid cells would be order 3×10^{20}, the number of macroparticles would be about 10^{23} and the time step would be limited to $\Delta x/c = 0.3$ μs. Doing 1 h of simulation would require 10^{33} particle pushes. Each particle push requires the order of 100 floating point operations (including the interpolation of the fields to the particle positions), so even on a future exascale computer which can do 10^{18} operations per second, this single simulation would take 10^{17} s wall clock time or about 3 billion years. Clearly, waiting for faster computers will not make such a simulation possible. One can switch to an implicit PIC code that requires resolving the electron skin depth (instead of the Debye length) that is about 1.5 km and the time step is restricted by the cell crossing time at the electron thermal speed instead of the speed of light. Reducing the ion-electron mass ratio from 1,836 to 100 results in another factor of ≈4 increase in the cell size to $\Delta x = 6\,\text{km} \approx 1/1,000\, R_E$, while the time step increases by a factor of about 6,000 relative to the explicit PIC code with realistic electron mass to $\Delta t \approx 2$ ms, which in turn reduces the computational cost by a factor of 10^9 to 3 years on the future exascale machine. The MHD-EPIC algorithm allows restricting the PIC code to the vicinity of the reconnection region(s), while one can use an adaptive grid for the global MHD code. The speedup is approximately the ratio of the volume of the PIC region relative to the whole domain, which is about 10^3. This reduces the computational cost to 1 day on a future exascale computer, which is promising, or about 3 years on a current petascale machine, still out of reach for now. With the kinetic scaling presented in this paper, however, the simulation becomes feasible. Using a scaling factor $f = 32$ allows 32 times coarser grid size of about $\Delta x = 200\,\text{km} = 1/32\, R_E$ and 32 times larger time step $\Delta t \approx 0.06$ s. This saves $f^4 \approx 10^6$, which makes the simulation doable in a few days using a few thousand cores (instead of a full petascale machine) with a code that in practice can only achieve a fraction of the peak performance. Our companion paper by Chen et al. (2017) does in fact present a 1 h long 3-D magnetosphere simulation using the MHD-EPIC model with kinetic scaling that was obtained with 6,400 cores of the Blue Waters computer running for a week.

In general, with proper kinetic scaling, the cost of the computation depends on the smallest global scales rather than on the true kinetic scales. Our simulations suggested that one can get reasonably accurate results with a scaled up inertial length d_i that is about 3% of the global scale d_g. Resolving the increased ion inertial length scale requires a grid resolution $\Delta x \approx d_i/10 \approx d_g/300$. This is much finer than the typical grids used in global MHD simulations that typically resolve the global scale with order 20 to 50 cells, but still achievable on current computers. Roughly speaking, kinetic simulations will require a grid resolution that is about 10 times finer than the grids used in MHD simulations, and the time step will also be about 10 times smaller. The computational cost of a 3-D simulation is proportional to $\Delta x^{-3}\Delta t^{-1}$, so this a factor of 10,000 increase. In two spatial dimensions the cost is proportional to the third power, or about a factor of 1,000. In addition, kinetic simulations are more expensive than MHD simulations on the same grid. The use of adaptive mesh refinement can reduce this cost substantially, because the high resolution is only needed in a relatively small region. Further efficiency gain can be achieved by using the MHD-EPIC algorithm, so that the PIC model is limited to the vicinity of the reconnection site. In summary, even with the scaling, kinetic simulations are much more expensive than ideal or resistive MHD simulations, but much more affordable than trying to resolve the true kinetic scales that may be many orders of magnitude smaller.

In contrast with pure MHD or pure PIC models, the MHD-EPIC approach combined with the kinetic scaling allows studying

1. kinetic dynamics embedded into a realistic and possibly time-dependent global environment, and
2. the self-consistent feedback of the kinetic solution on the global dynamics.

Studying collisionless reconnection in global systems allows, for example, direct comparison of full electron and ion distribution functions with observations, such as those provided by the MMS mission. Self-consistent MHD-EPIC simulations can get correct collisionless reconnection rates and global dynamics based on electron physics instead of numerical resistivity. This may lead to a better understanding of the mechanisms producing magnetospheric substorms and solar eruptions, for example.

This paper focused on the kinetic scaling and demonstrated it with 2-D simulations. We have already performed 3-D MHD-EPIC simulations for Earth's magnetosphere using scaling factors $f = 16$ and $f = 32$.

The results of these simulations are discussed in an accompanying paper by Chen et al. (2017) showing several kinetic effects predicted and observed in the dayside magnetosphere including flux transfer events, Larmor electric field, the lower hybrid drift instability, and crescent shape velocity distribution functions. Our 2-D and 3-D simulations focused on various aspects of the reconnection process at the dayside magnetopause and found that the kinetic scaling works for these. It will require further research to examine if these results generalize to other aspects (like particle acceleration), other parameter regimes (reconnection in solar flares), and other type of kinetic processes (for example, kinetic instabilities at parallel shocks).

Acknowledgments
This research was partially supported by INSPIRE NSF grant PHY-1513379, by the NSF/NASA LWS Strategic Capabilities grant AGS-1322543, and by the Space Hazards Induced near Earth by Large, Dynamic Storms (SHIELDS) and the Impacts of Extreme Space Weather Events on Power Grid Infrastructure projects funded by the U.S. Department of Energy (DE-AC52-06NA25396) through the Los Alamos National Laboratory Directed Research and Development program. Paul Cassak was supported by NASA grant NNX16AF75G. Computational resources supporting this work were provided on the Blue Waters super computer by the NSF PRAC grant ACI-1640510, on the Pleiades computer by NASA High-End Computing (HEC) Program through the NASA Advanced Supercomputing (NAS) Division at Ames Research Center, and from Yellowstone (ark:/85065/d7wd3xhc) provided by NCAR's Computational and Information Systems Laboratory, sponsored by the National Science Foundation. The SWMF code (including BATS-R-US and iPIC3D) is publicly available through the csem.engin.umich.edu/tools/swmf website after registration. The output of the simulations presented in this paper can be obtained by contacting the first author G. T.

References

Birn, J., Drake, J. F., Shay, M. A., Rogers, B. N., Denton, R. E., Hesse, M., … Pritchett, P. L. (2001). Geospace Environmental Modeling (GEM) magnetic reconnection challenge. *Journal of Geophysical Research*, *106*(A3), 3715–3720. https://doi.org/10.1029/1999JA900449

Boris, J. P. (1970). A physically motivated solution of the ALfvén problem (Tech. Rep. NRL Memorandum Report 2167). Washington, DC: Naval Research Laboratory.

Brackbill, J., & Forslund, D. (1982). An implicit method for electromagnetic plasma simulation in two dimensions. *Journal of Computational Physics*, *46*, 271–308. https://doi.org/10.1016/0021-9991(82)90016-X

Cassak, P. A., & Shay, M. A. (2007). Scaling of asymmetric magnetic reconnection: General theory and collisional simulations. *Physics of Plasmas*, *14*, 102114. https://doi.org/10.1063/1.2795630

Chen, Y., Tóth, G., Cassak, P., Jia, X., Gombosi, T. I., Slavin, J., … Henderson, M. G. (2017). Global three-dimensional simulation of Earth's dayside reconnection using a two-way coupled magnetohydrodynamics with embedded particle-in-cell model: Initial results. *Journal of Geophysical Research*, *122*. https://doi.org/10.1002/2017JA024186

Daldorff, L. K. S., Tóth, G., Gombosi, T. I., Lapenta, G., Amaya, J., Markidis, S., & Brackbill, J. U. (2014). Two-way coupling of a global Hall magnetohydrodynamics model with a local implicit particle-in-cell model. *Journal of Computational Physics*, *268*, 236–254. https://doi.org/10.1016/j.jcp.2014.03.009

Dedner, A., Kemm, F., Kröner, D., Munz, C., Schnitzer, T., & Wesenberg, M. (2003). Hyperbolic divergence cleaning for the MHD equations. *Journal of Computational Physics*, *175*, 645–673.

Dorelli, J. C., Glocer, A., Collinson, G., & Toth, G. (2015). The role of the hall effect in the global structure and dynamics of planetary magnetospheres: Ganymede as a case study. *Journal of Geophysical Research: Space Physics*, *120*, 5377–5392. https://doi.org/10.1002/2014JA020951

Gombosi, T. I., Tóth, G., De Zeeuw, D. L., Hansen, K. C., Kabin, K., & Powell, K. G. (2002). Semirelativistic magnetohydrodynamics and physics-based convergence acceleration. *Journal of Computational Physics*, *177*, 176–205. https://doi.org/10.1006/jcph.2002.7009

Hesse, M., Schindler, K., Birn, J., & Kuznetsova, M. (1999). The diffusion region in collisionless magnetic reconnection. *Physics of Plasmas*, *6*, 1781–1795. https://doi.org/10.1063/1.873436

Huba, D., & Rudakov, L. (2004). Hall magnetic reconnection rate. *Physical Review Letters*, *93*, 175003. https://doi.org/10.1103/PhysRevLett.93.175003

Koren, B. (1993). A robust upwind discretisation method for advection, diffusion and source terms. In C. Vreugdenhil, & B. Koren (Eds.), *Numerical Methods for Advection-Diffusion Problems* (pp. 117). Braunschweig: Vieweg.

Lapenta, G., Markidis, S., Divin, A., Goldman, M., & Newman, D. (2010). Scales of guide field reconnection at the hydrogen mass ratio. *Physics of Plasmas*, *17*(8), 82106. https://doi.org/10.1063/1.3467503

Liu, Y.-H., Hesse, M., Guo, F., Daughton, W., Li, H., Cassak, P. A., & Shay, M. A. (2017). Why does steady-state magnetic reconnection have a maximum local rate of order 0.1? *Physical Review Letters*, *118*, 85101. https://doi.org/10.1103/PhysRevLett.118.085101

Markidis, S., Lapenta, G., & Uddin, R. (2010). Multi-scale simulations of plasma with iPIC3D. *Mathematics and Computers in Simulation*, *80*, 1509–1519. https://doi.org/10.1016/j.matcom.2009.08.038

Mozer, F. S., & Hull, A. (2010). Scaling the energy conversion rate from magnetic field reconnection to different bodies. *Physics of Plasmas*, *17*, 102906. https://doi.org/10.1063/1.3504224

Nitta, S., Tanuma, S., & Maezawa, K. (2002). A self-similar solution of fast magnetic reconnection: A semianalytic study of the inflow region. *Astrophysical Journal*, *580*, 538–549. https://doi.org/10.1086/343067

Powell, K. G. (1994). An approximate Riemann solver for magnetohydrodynamics (that works in more than one dimension) (Tech. Rep. 94-24). Hampton, VA: Institute for Computation Applied in Science and Engineering, NASA Langley Space Flight Center.

Powell, K., Roe, P., Linde, T., Gombosi, T., & De Zeeuw, D. L. (1999). A solution-adaptive upwind scheme for ideal magnetohydrodynamics. *Journal of Computational Physics*, *154*, 284–309. https://doi.org/10.1006/jcph.1999.6299

Ricci, P., Brackbill, J. U., Daughton, W., & Lapenta, G. (2004). Collisionless magnetic reconnection in the presence of a guide field. *Physics of Plasmas*, *11*, 4102–4114.

Rusanov, V. V. (1962). The calculation of the interaction of non-stationary shock waves and obstacles. *USSR Computational Mathematics and Mathematical Physics*, *1*, 304–320. https://doi.org/10.1016/0041-5553(62)90062-9

Schoeffler, K. M., Drake, J. F., & Swisdak, M. (2012). Scaling of the growth rate of magnetic islands in the heliosheath. *The Astrophysical Journal Letters*, *750*(2), L30. https://doi.org/10.1088/2041-8205/750/2/L30

Shay, M. A., & Drake, J. F. (1998). The role of electron dissipation on the rate of collisionless magnetic reconnection. *Geophysical Research Letters*, *25*, 3759–3762. https://doi.org/10.1029/1998GL900036

Shay, M., Drake, J., Rogers, B., & Denton, R. (1999). The scaling of collisionless, magnetic reconnection for large systems. *Geophysical Research Letters*, *26*, 2163–2166. https://doi.org/10.1029/1999GL900481

Shay, M. A., Drake, J. F., & Swisdak, M. (2007). Two-scale structure of the electron dissipation region during collisionless magnetic reconnection. *Physical Review Letters*, *99*, 155002. https://doi.org/10.1103/PhysRevLett.99.155002

Shibata, K., & Tanuma, S. (2001). Plasmoid-induced-reconnection and fractal reconnection. *Earth, Planets and Space*, *53*, 473–482. https://doi.org/10.1186/BF03353258

Tenerani, A., Velli, M., Rappazzo, A. F., & Pucci, F. (2015). Magnetic reconnection: Recursive current sheet collapse triggered by "ideal" tearing. *The Astrophysical Journal Letters*, *813*, L32. https://doi.org/10.1088/2041-8205/813/2/L32

Tóth, G., Jia, X., Markidis, S., Peng, B., Chen, Y., Daldorff, L., … Dorelli, J. (2016). Extended magnetohydrodynamics with embedded particle-in-cell simulation of Ganymede's magnetosphere. *Journal of Geophysical Research: Space Physics*, *121*, 1273–1293. https://doi.org/10.1002/2015JA021997

Tóth, G., Ma, Y. J., & Gombosi, T. I. (2008). Hall magnetohydrodynamics on block adaptive grids. *Journal of Computational Physics*, *227*, 6967–6984. https://doi.org/10.1016/j.jcp.2008.04.010

Tóth, G., Sokolov, I. V., Gombosi, T. I., Chesney, D. R., Clauer, C., Zeeuw, D. L. D., … (2005). Space weather modeling framework: A new tool for the space science community. *Journal of Geophysical Research*, *110*, A12226. https://doi.org/10.1029/2005JA011126

Tóth, G., van der Holst, B., Sokolov, I. V., Zeeuw, D. L. D., Gombosi, T. I., Fang, F., … Opher, M. (2012). Adaptive numerical algorithms in space weather modeling. *Journal of Computational Physics*, *231*, 870–903. https://doi.org/10.1016/j.jcp.2011.02.006

van Leer, B. (1979). Towards the ultimate conservative difference scheme. V. A second-order sequel to Godunov's method. *Journal of Computational Physics*, *32*, 101–136.

Vasyliunas, V. (1975). Theoretical models of magnetic field line merging, 1. *Reviews of Geophysics*, *13*, 303–336.